AIAA JOURNAL
Vol. 30, No. 8, August 1992

Interaction Between Crossing Oblique Shocks and a Turbulent Boundary Layer

N. Narayanswami* and D. Knight†
Rutgers University, Piscataway, New Jersey 08855
S. M. Bogdonoff‡
Princeton University, Princeton, New Jersey 08540
and
C. C. Horstman§
NASA Ames Research Center, Moffett Field, California 94035

A numerical study of the three-dimensional interaction between crossing shocks generated by symmetric sharp fins and a flat-plate turbulent boundary layer is presented. The full mean compressible Navier-Stokes equations, incorporating a turbulent eddy-viscosity model, are solved. Computed results for the flow past (11 deg, 11 deg) symmetric fins at a freestream Mach number $M_\infty = 2.95$ and Reynolds number $Re_{\delta_\infty} = 2.5 \times 10^5$ (based on the undisturbed boundary-layer thickness δ_∞) show general agreement with experimental measurements for flat-plate surface pressure and surface flow visualization. Analysis of the computed flowfield reveals a complex interaction involving the "collision" of two slowly counter-rotating vortical structures generated by the initial shock/boundary-layer interaction due to each fin. Associated with the streamline structure of the interaction is the formation and growth of a region of low energy near the centerline, downstream of the crossed shocks. A "first look" at the shock structure of the interaction is provided.

Introduction

THE three-dimensional interaction between shock waves and turbulent boundary layers (denoted as "three-dimensional turbulent interactions") is an important research problem in the area of high-speed flows that has a variety of applications in aerodynamics, propulsion, gas-dynamic lasers, and turbomachinery. Flows over aircraft wing-body junctures and control surfaces and within high-speed inlets are typical examples in which the interactions are of interest. Research has focused primarily on the understanding of the flowfield structure of three-dimensional turbulent interactions due to simple shock generator geometries that represent practical (more complex) aerodynamic configurations. Recent reviews are presented in Settles and Dolling[1] and Zheltovodov et al.[2]

The present study focuses on an interaction problem that has direct application to the design of air-breathing aircraft inlet systems. One of the primary goals of high-speed inlet design is to effectively control three-dimensional turbulent interactions in order to provide the engine with nearly uniform, high total pressure flow. Flow separation and unsteadiness can result in significant nonuniformities and substantial loss of total pressure that can be detrimental to the operation of the engine. Hence, proper understanding of turbulent interactions in the supersonic portion of the inlet is essential to the development of an efficient propulsion system. A "simplified" geometry such as two sharp fins mounted on a flat plate (Fig. 1), representing a generic high-speed inlet configuration, provides the opportunity to study the three-dimensional interaction between the crossing oblique shocks generated due to the fins and the turbulent boundary layer on the flat plate.

A preliminary numerical study of the three-dimensional crossing shock problem for such a configuration was con-

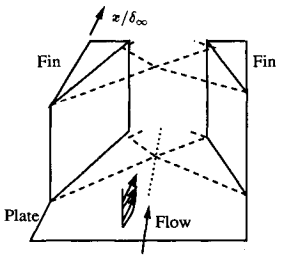

Experimental Domain

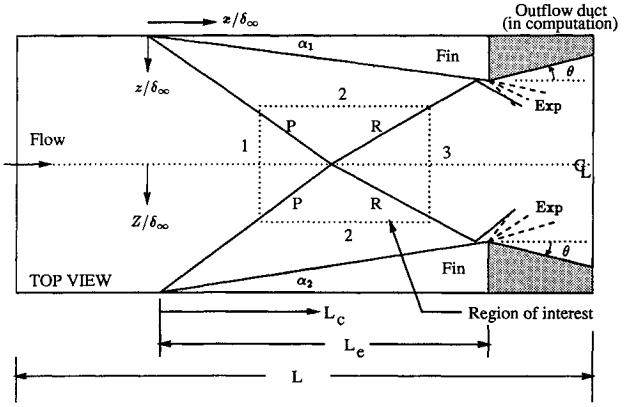

Experimental and Computational Domain

Fig. 1 Crossing shock interaction, experimental and computational domain. P = primary shock R = reflected shock, Exp = expansion, and θ = outflow duct angle (in computation).

Presented as Paper 91-0649 at the AIAA 29th Aerospace Sciences Meeting, Reno, NV, Jan. 7-10, 1991; received June 18, 1991; revision received Jan. 9, 1992; accepted for publication Jan. 10, 1992.

*Graduate Research Assistant, Department of Mechanical and Aerospace Engineering. Student Member AIAA.

†Professor, Department of Mechanical and Aerospace Engineering. Associate Fellow AIAA.

‡Professor Emeritus, Senior Research Scholar, Department of Mechanical and Aerospace Engineering. Fellow AIAA.

§Senior Scientist. Associate Fellow AIAA.

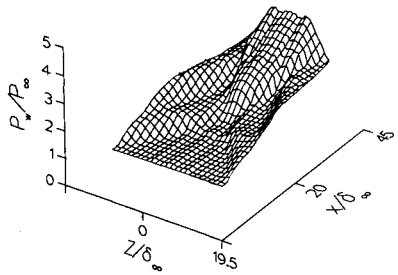

Fig. 2a Experimental flat-plate surface pressure (P/P_∞) distribution.

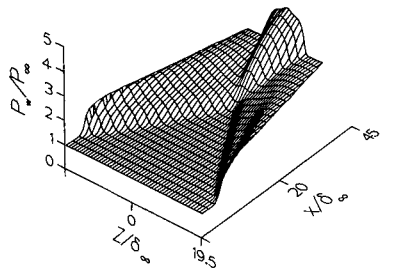

Fig. 2b Computed flat-plate surface pressure (P/P_∞) distribution (Baldwin-Lomax model).

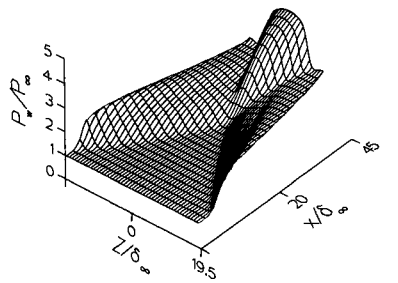

Fig. 2c Computed flat-plate surface pressure (P/P_∞) distribution (k-ϵ model).

ducted by Gaitonde[3] for fin angles (α_1, α_2) = (5 deg, 5 deg) at Mach 1.85 and (4 deg, 4 deg) and (8 deg, 8 deg) at Mach 2.95. Comparison of computed results for the (5 deg, 5 deg) interaction with the experimental data of Mee[4] showed overall good agreement; however, the interaction was weak and unseparated (based on the surface streamline pattern and Lighthill's criteria for separation[5]). No experimental results were available for the stronger (Mach 2.95) interactions at the time of the study. Recent experiments by Batcho et al.[6] have examined the crossing shock interaction for a range of fin angles at Mach 2.95. Mean and fluctuating surface pressure measurements and surface flow visualization reveal a complex flowfield particularly in the vicinity of the shock crossing location. The present research effort is aimed at further investigating the flowfield structure of this interaction. The flow past (9 deg, 9 deg) and (11 deg, 11 deg) symmetric fin configurations are simulated numerically and the computed results compared with the experimental data of Batcho et al.[6]

Flow Conditions

The flow conditions for the three-dimensional crossing shock experiments of Batcho et al.[6] are a freestream Mach number $M_\infty = 2.95$, Reynolds number $Re_{\delta_\infty} = 2.5 \times 10^5$, and adiabatic walls. The two-dimensional incoming turbulent boundary layer was self-preserving, and the velocity profile satisfied the law of the wall and wake.[7] The undisturbed boundary-layer thickness δ_∞ near the fin leading-edge location was approximately 0.4 cm.

Table 1 Details of computed cases[a] (reference Fig. 1) (11 deg, 11 deg) interaction

Case	L_c/δ_∞	θ	Turbulence model
A	61.0	0 deg	Baldwin-Lomax
B	61.0	20 deg	Baldwin-Lomax
C	61.0	0 deg	Jones-Launder
D	47.0	None ($L_c < L_e$)	Baldwin-Lomax

[a] L_c = length of computational domain; L_e = length of experimental domain; δ_∞ = upstream boundary layer thickness; and θ = outflow duct angle (in computation).

Details of Computations

Computations have been performed by Narayanswami and Horstman for the (11 deg, 11 deg) interaction, using two different turbulence models and for flow conditions identical to the experiment. Additional computations, performed for the (9 deg, 9 deg) interaction by Narayanswami, are discussed in Ref. 8.

Theoretical Model

The theoretical model is the full three-dimensional mean compressible Reynolds-averaged Navier-Stokes equations in strong conservation form.[9] The molecular and turbulent Prandtl numbers are 0.73 and 0.9, respectively, with molecular viscosity specified by Sutherland's law. The computations by Narayanswami incorporate the Baldwin-Lomax[10] two-layer algebraic turbulent eddy-viscosity model. The constants C_{cp} and C_{kleb} in the "outer" eddy-viscosity formulation are 2.08 and 0.3, respectively. The value of C_{cp} is 30% higher than originally proposed by Baldwin and Lomax and is based upon previous single-fin interaction studies[11] at Mach 3. The remaining constants in the eddy-viscosity formulation are not modified. The computation by Horstman incorporates the Jones-Launder[12] two-equation (k-ϵ) turbulent eddy-viscosity model.

Boundary Conditions

Utilizing the experimental flowfield symmetry in the vertical and spanwise directions, the physical domain of the computations is reduced to one-fourth the experimental domain. A boundary-fitted coordinate transformation (ξ, ζ, η) is employed.[13] On the inflow boundary, the two-dimensional incoming equilibrium turbulent boundary-layer profile is prescribed. On the flat-plate and fin surfaces, the velocity vector, turbulent kinetic energy k, rate of dissipation of turbulent kinetic energy ϵ, and the normal gradient of static pressure are set to zero. The temperature is set to the adiabatic wall temperature. On the symmetry boundaries (i.e., top and side surfaces), the normal component of velocity is set to zero and the normal derivatives of the remaining velocity components, static pressure, temperature, k and ϵ are set to zero. A zero-gradient extrapolation condition is imposed on the outflow boundary.

Numerical Algorithm

The computations by Narayanswami employ the hybrid explicit-implicit scheme of Knight.[13] The full Navier-Stokes equations are integrated on an "ordinary" grid which is interfaced with a "viscous sublayer" grid, adjacent to solid surfaces, on which the asymptotic form of the Navier-Stokes equations are employed. The ordinary grid points are updated using the explicit scheme of MacCormack[14] whereas the viscous sublayer grid is updated using the Keller[15] box implicit method. The computation by Horstman employs the hybrid scheme of MacCormack.[16]

Computational Domain and Grid Details

Details of the computations are presented in Tables 1–3. The experimental geometry (Fig. 1), incorporated straight fins

of length $L_e = 56\delta_\infty$. To simplify the structure of the body-fitted curvilinear coordinates in the vicinity of the fin trailing edge, the flow geometry for cases A, B, and C was extended to a distance L_c by adding a section with divergence angle θ. This modification was verified a posteriori to have no significant effect on the computed flowfield within the region of experimental measurements (i.e., $x < L_e$). This result is consistent with the observation that the computed outflow was supersonic almost everywhere. A fourth computation (case D) was performed with the domain length $L_c = 47\delta_\infty = 0.84L_e$ to provide additional confirmation of the independence of the computed flowfield within the crossed shock region to the outflow boundary conditions.

The inflow boundary was chosen at a streamwise position $5\delta_\infty$ upstream of the fin leading-edge location. This distance has been employed in several three-dimensional single fin studies.[3,11,13] In all cases (including all computations in the present study), the changes in the values of the flow variables in the first two or three planes have been found to be either zero or less than 0.1%, thus indicating that the inflow boundary is well upstream of the interaction. The boundary-layer profile on the inflow plane was obtained by computing a flat-plate turbulent boundary layer (using the appropriate turbulence model) to a point where the computed δ_∞ was equal to the experimental value (0.4 cm). In addition, the velocity profiles of both experiment and computation showed close agreement with the law of the wall and wake.[7]

The grid systems used in each computation were generated following the technique employed in previous three-dimensional single fin computations by Knight[11,13,17] and Horstman.[18,19] Details of the grid systems are given in Tables 2 and 3. A uniformly spaced grid is employed in the streamwise (x) direction. In the cross-flow (y and z) directions, the grids are nonuniform and are generated algebraically using simple geometric stretching. The height of the first grid point adjacent to the flat-plate/fin surfaces (i.e., the minimum grid spacings) are $1.3 \times 10^{-4}\delta_\infty$ and $2.16 \times 10^{-4}\delta_\infty$, respectively for cases A, B, and D, and $1.47 \times 10^{-4}\delta_\infty$ and $1.25 \times 10^{-3}\delta_\infty$, respectively, for case C. The maximum grid spacings in each case occur in the freestream regions. The grid density in a typical crossflow

Table 2 Details of grid[a]

					$\Delta y/\delta_\infty$		$\Delta z/\delta_\infty$		
Case	N_ξ	N_ζ	N_η	$\Delta x/\delta_\infty$	Min	Max	Min	Max	*NBL*
A	67	42	54	1.0	1.30×10^{-4}	0.725	2.16×10^{-4}	0.635	23
B	67	42	54	1.0	1.30×10^{-4}	0.725	2.16×10^{-4}	0.635	23
C	64	40	64	1.0	1.47×10^{-4}	0.629	1.25×10^{-3}	0.402	23
D	53	42	54	1.0	1.30×10^{-4}	0.725	2.16×10^{-4}	0.635	23

[a] N_ξ, N_ζ, N_η = number of grid points in ξ, ζ, and η directions, respectively; Δx, Δy, Δz = grid spacings in the x, y, and z directions, respectively; δ_∞ = upstream boundary-layer thickness, *NBL* = number of grid points in flat-plate boundary layer (typical), Min = minimum; and Max = maximum.

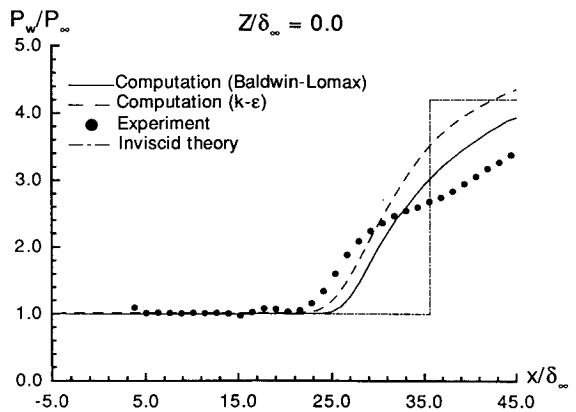

Fig. 3a Flat-plate surface pressure (P/P_∞) along interaction centerline.

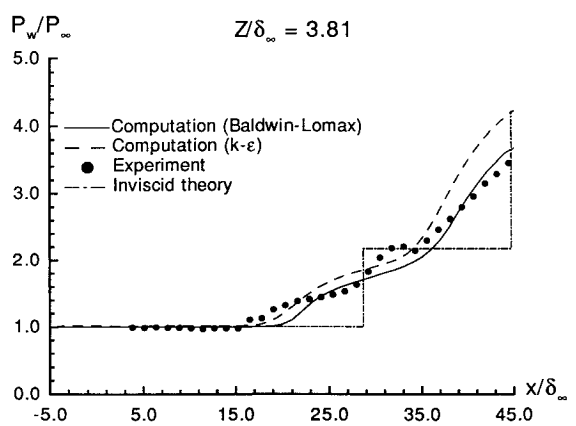

Fig. 3b Flat-plate surface pressure (P/P_∞) along $Z/\delta_\infty = 3.81$.

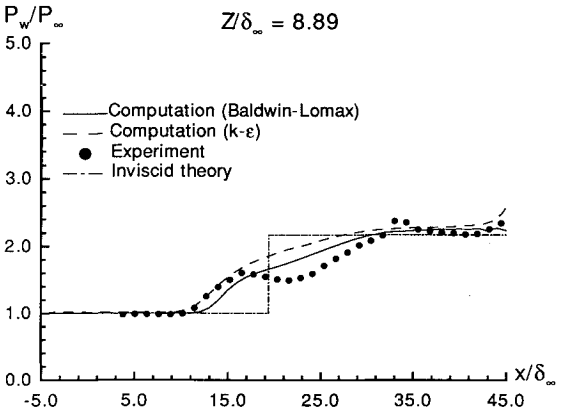

Fig. 3c Flat-plate surface pressure (P/P_∞) along $Z/\delta_\infty = 8.89$.

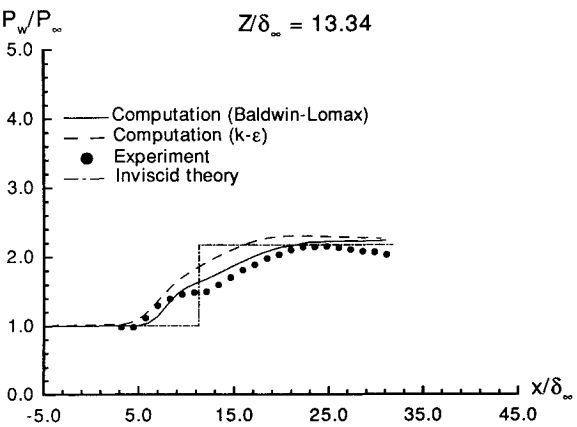

Fig. 3d Flat-plate surface pressure (P/P_∞) along $Z/\delta_\infty = 13.3$.

Table 3 Resolution of viscous sublayer[a]

	Δy^+		y^+		Δz^+		z^+	
Case	Avg	Max	Avg	Max	Avg	Max	Avg	Max
A,B,D	0.36	0.67	11.52	21.58	0.68	0.94	21.79	30.14
C	0.30	1.0	N/A	N/A	1.6	3.0	N/A	N/A

[a] Δy^+ = height of first point adjacent to flat plate in wall units, y^+ = height of computational sublayer on flat plate in wall units; Δz^+ = height of first point adjacent to fin surface in wall units; z^+ = height of computational sublayer on fin surface in wall units, N/A = not applicable; Avg = average; Max = maximum; and "wall units" implies normalization by the local viscous length scale ν_w/u^*.

plane is thus maximum in the region adjacent to the solid surfaces and minimum in the freestream (inviscid) regions.

Accurate resolution of the flowfield was achieved in all computations. First, the grid points adjacent to the flat plate satisfied $\Delta y^+ \leq 1.0$ at all locations, where $\Delta y^+ = \Delta y\, u^*/\nu_w$, $u^* = \sqrt{\tau_w/\rho_w}$ is the local friction velocity, τ_w is the wall shear stress, ρ_w is the density at the wall, and ν_w is the kinematic viscosity at the wall. The average value of Δy^+ was 0.30 to 0.36 depending on the case. The corresponding maximum values for the first point adjacent to the fin surface are $\Delta z^+ = 0.94$ for cases A, B, D and $\Delta z^+ = 3.0$ for case C, respectively, and the average values are $\Delta z^+ = 0.68$ and 1.6. Second, the height of the computational sublayer (applicable to cases A, B, and D only) adjacent to the flat plate and the fin satisfied $y^+ \leq 21.6$ and $z^+ \leq 30.1$, respectively, which are well within the requirement[13] $y^+ \leq 60$ and $z^+ \leq 60$. Third, a total of 23 points were typically contained within the boundary layer on the flat plate, thereby satisfying the criteria, established in previous three-dimensional turbulent interaction computations,[17-21] of a minimum of 20 points within the boundary layer. Fourth, the maximum crossflow grid spacing in the y and z directions ($\Delta y_{max}/\delta_\infty = 0.725$ and $\Delta z_{max}/\delta_\infty = 0.635$) is comparable to the typical maximum crossflow grid spacing $0.7\delta_\infty$ employed in three-dimensional turbulent interaction computations to date.[17-21] A recent study by Knight and Badekas[22] for a three-dimensional single-fin interaction at Mach 4 has shown that adequate resolution of the flowfield is achievable with such maximum crossflow grid spacing, and that further refinement of the maximum crossflow grid spacing provides a sharper definition of the shock structure. Fifth, the streamwise grid spacing $\Delta x/\delta_\infty = 1.0$ has been found to be adequate in previous studies by Knight[11,17,21] for three-dimensional single-fin interactions.

Initial Conditions and Convergence

The initial condition for all computations was obtained by extending the two-dimensional upstream boundary-layer profile to all downstream stations. Convergence of the flowfield to a steady state was determined[13] by monitoring the absolute relative change of the flow variables over a physical time of $1T_c$, where T_c is the time required for a fluid parcel to travel the streamwise length of the domain in the freestream. At convergence, the relative change in the flow variables such as ρ, ρu, and ρe over this time span was less than 1% at all locations. Here, ρ denotes the density of the fluid and u and e denote the streamwise component of velocity and total energy per unit mass, respectively. Furthermore, the maximum relative change in the surface pressure and skin-friction distributions at convergence was also less than 1% in each case. Each computation typically involved iteration up to a physical time of approximately $4.5\text{-}5.0T_c$ to reach steady state.

Results

Results for the (11 deg, 11 deg) configuration are presented below. Results for the (9 deg, 9 deg) cases were found to be qualitatively similar to the (11 deg, 11 deg) cases and are discussed in Ref. 8. Note for reference that in Figs. 2-7, the coordinate "Z" represents distance measured away from the interaction centerline ($Z = 0$) in a spanwise direction.

Effect of Outflow Geometry

A comparison of the computed results in cases A, B, and D was made to ascertain the effect of the outflow divergence angle θ. It was found that up to a streamwise distance of approximately $45.0\delta_\infty$ downstream of the fin leading edges, the average absolute relative difference in the values of Mach number and static, total, and pitot pressures between the three cases was $\leq 1\%$ at any given streamwise location. The shock waves intersect at $x/\delta_\infty \approx 34.0$. It is thus concluded that the computed flowfields are independent of the outflow conditions up to $x/\delta_\infty = 45.0$. The present study focuses, therefore, on comparison with experiment and development of the flowfield model in the region $x \leq 45.0\delta_\infty$.

Comparison with Experiment

Available experimental data for the symmetric fin configurations includes flat-plate surface pressure measurements obtained using static pressure orifices spanning the interaction region. The distance between the orifice centers is 0.1 in. ($0.635\delta_\infty$). Surface streamline patterns were also obtained on the flat plate using the kerosene-lampblack technique.

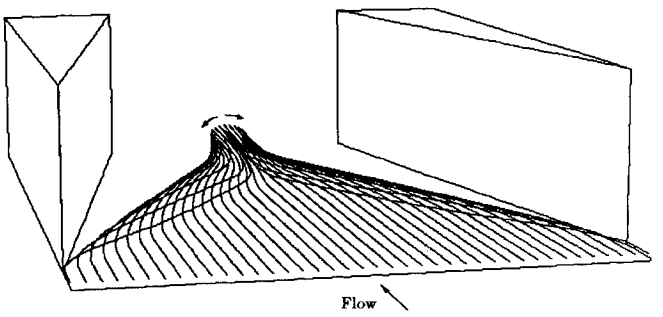

Fig. 4a Streamlines originating at $y/\delta_\infty = 0.25$ in upstream boundary layer (Baldwin-Lomax model).

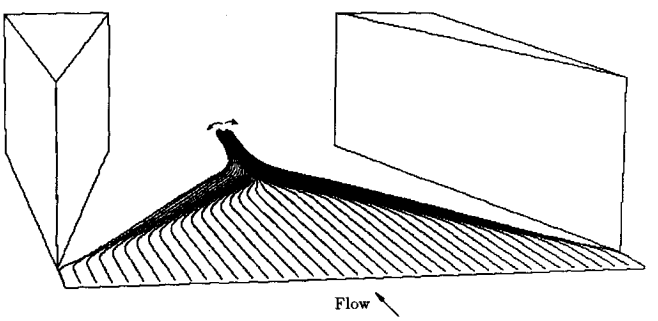

Fig. 4b Streamlines originating at $y/\delta_\infty = 0.01$ in upstream boundary layer (Baldwin-Lomax model).

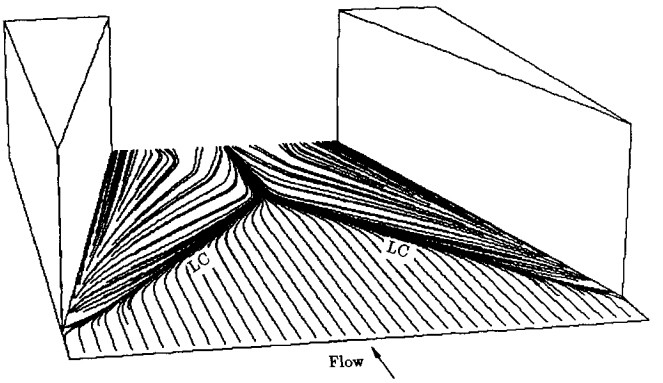

Fig. 4c Surface (limiting) streamline pattern (Baldwin-Lomax model). LC = line of coalescence.

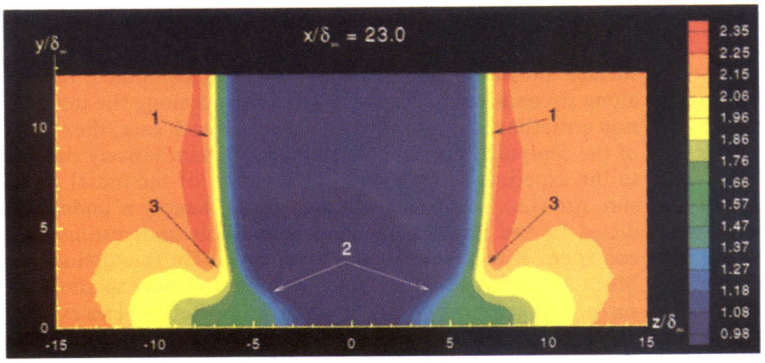

Fig. 5a Static pressure contours on crossflow (y-Z) plane at $x/\delta_\infty = 23.0$ (Baldwin-Lomax model). 1 = primary shock; 2 = separation shock; and 3 = rear shock.

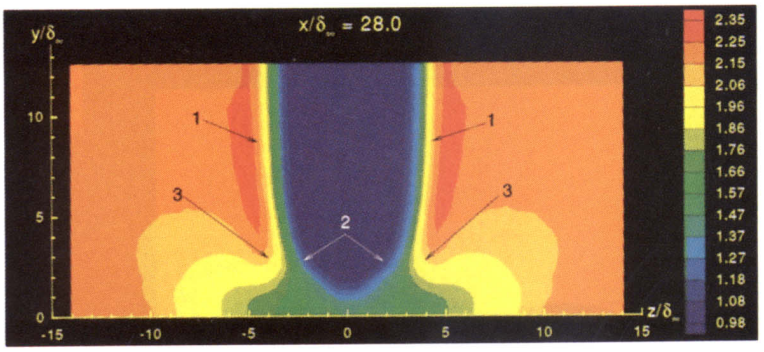

Fig. 5b Static pressure contours on crossflow (y-Z) plane at $x/\delta_\infty = 28.0$ (Baldwin-Lomax model). 1 = primary shock; 2 = separation shock; and 3 = rear shock.

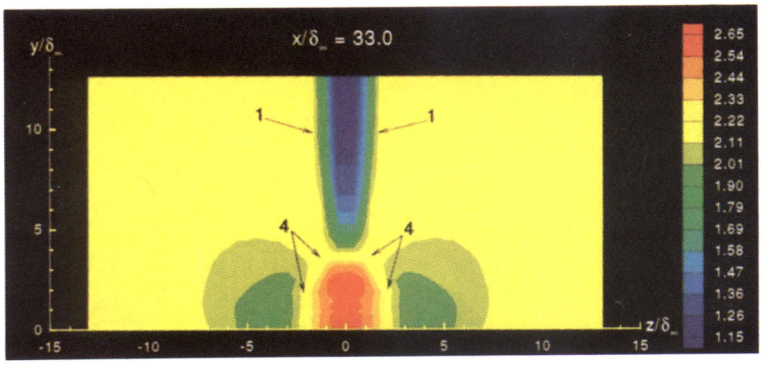

Fig. 5c Static pressure on crossflow (y-Z) plane at $x/\delta_\infty = 33.0$ (Baldwin-Lomax model). 1 = primary shock; 4 = shock.

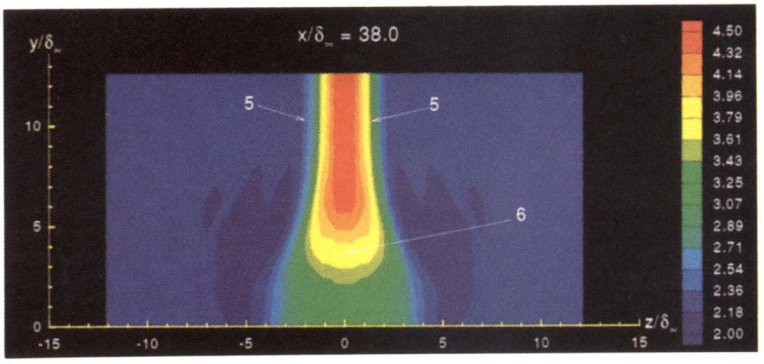

Fig. 5d Static pressure on crossflow (y-Z) plane at $x/\delta_\infty = 38.0$ (Baldwin-Lomax model). 5 = reflected shock; 6 = expansion.

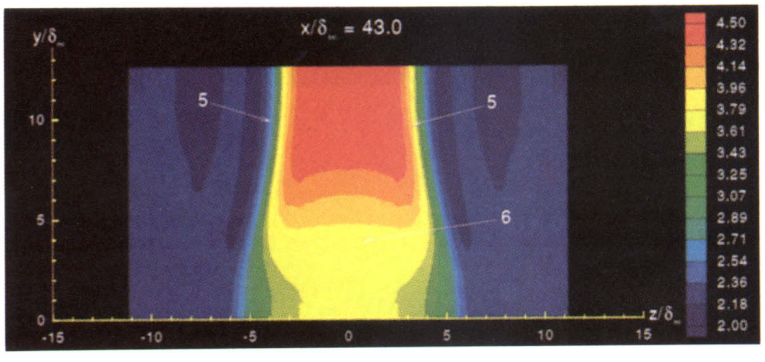

Fig. 5e Static pressure on crossflow (y-Z) plane at $x/\delta_\infty = 43.0$ (Baldwin-Lomax model). 5 = reflected shock; 6 = expansion.

The computed and experimental surface pressures are compared in Figs. 2a–2c. The results for the two different turbulence models show good agreement. There is general agreement between the computations and experiment with regard to the magnitude of pressure rise through the shocks although the shape of the pressure rise predicted by the computations appears somewhat sharper than that observed in the experiment. The spanwise distribution of surface pressure is not well captured by the computations particularly near the downstream boundary of the domain (i.e, near $x/\delta_\infty = 45.0$). This difference cannot be attributed to any upstream influence of outflow conditions since the flowfield up to $x/\delta_\infty = 45.0$ has been clearly shown to be independent of variations in outflow duct geometry. A more direct comparison of the experimental surface pressure measurements with the computed results along streamwise cuts taken parallel to and along the interaction centerline is shown in Figs. 3a–3d. In each case, the shape of the computed pressure distribution is quantitatively similar to the experiment. However, the location of the initial pressure rise (i.e., the extent of upstream influence) is underpredicted by the Baldwin-Lomax model. This underestimate is consistent with previous studies of single-fin interactions at Mach 3.[11,17,21] A discussion of the computed and experimental surface streamline patterns is provided in Ref. 8. The experi-

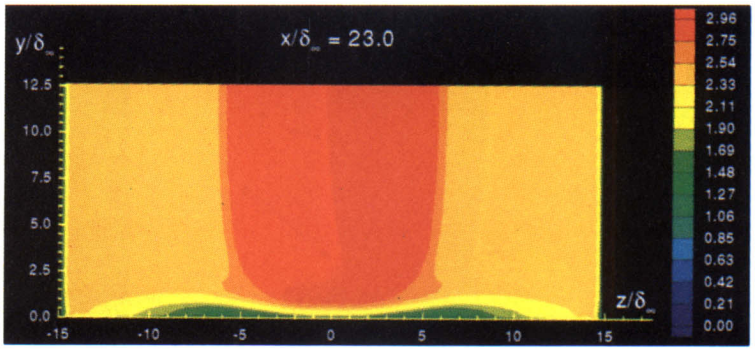

Fig. 6a Mach number on crossflow (y-Z) plane at $x/\delta_\infty = 23.0$ (Baldwin-Lomax model).

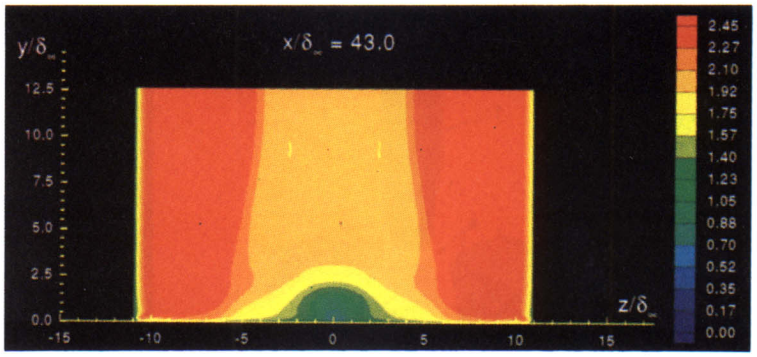

Fig. 6b Mach number on crossflow (y-Z) plane at $x/\delta_\infty = 43.0$ (Baldwin-Lomax model).

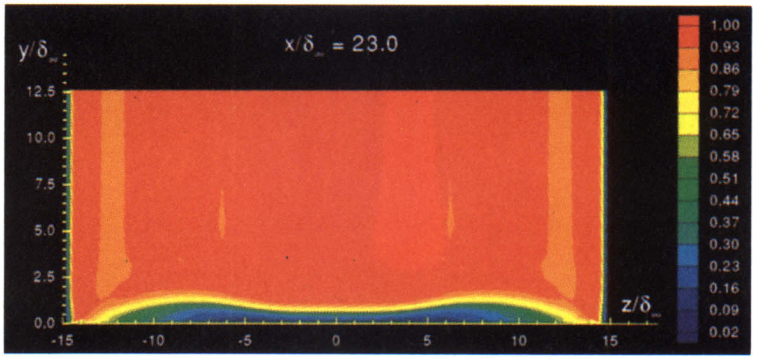

Fig. 7a Normalized total pressure (P_t/P_{t_∞}) on crossflow (y-Z) plane at $x/\delta_\infty = 23.0$ (Baldwin-Lomax model).

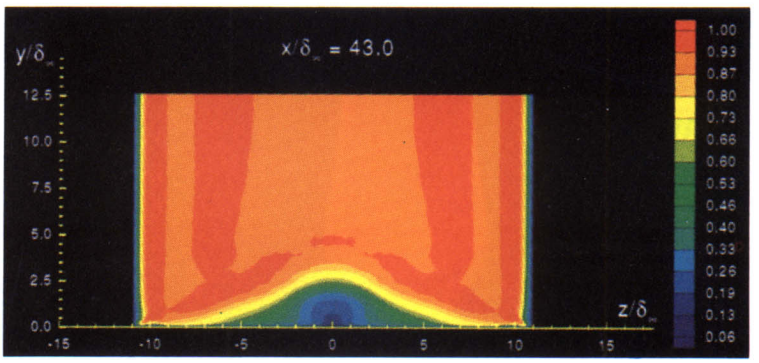

Fig. 7b Normalized total pressure (P_t/P_{t_∞}) on crossflow (y-Z) plane at $x/\delta_\infty = 43.0$ (Baldwin-Lomax model).

mental surface flow visualization for the (11 deg, 11 deg) case is incomplete in several places thus precluding a complete analysis of the surface flow topology.

Flowfield Streamline Structure

The flowfield streamline structure is analyzed using the computed results, recognizing that although the comparison between theory and experiment has demonstrated general agreement, there are, as discussed previously, some discrepancies. Because of the observed similarity of the computed results using the Baldwin-Lomax and k-ϵ models, results are shown for the Baldwin-Lomax model only.

Particles are released at various distances from the flat plate within and outside the incoming boundary layer and the trajectories of these particles examined. This technique has been successfully employed in the past to determine the streamline structure of the single-fin interaction.[11] Streamlines originating at levels of $y/\delta_\infty = 0.25$ and 0.01 are shown in Figs. 4a and 4b. Also, the "limiting" or "surface" streamline pattern is shown in Fig. 4c. The surface pattern shows the formation of two lines of coalescence (LC) that approach each other near the centerline. The formation of two counter-rotating vortical structures (one generated due to each fin) is evident from the traces originating at y/δ_∞ of 0.01 and 0.25. The sense of rotation of these structures (looking downstream) is "clockwise" on the right of the centerline and "counterclockwise" on the left of the centerline. Upstream of the interaction of the two vortical structures, the flow on each side of the geometric centerline is, as expected, similar to that for single-fin interactions. The "collision" of the two vortical structures at the centerline leads to a more complex flow pattern in the vicinity of the shock-shock intersection. A low-energy jet (comprised of the two slowly counter-rotating vortical structures) forms and rises sharply away from the flat plate due to the adverse pressure gradient encountered immediately downstream of the crossed shocks.

Flowfield Shock Structure

Figures 5a–5e show contours of computed static pressure (P/P_∞) on five crossflow (y-Z) planes for the flowfield computed using the Baldwin-Lomax model. Comparable results were obtained for the k-ϵ model. The five planes represent the locations $x/\delta_\infty = 23.0$, 28.0 (both upstream of the shock crossing location), 33.0 (immediately upstream of the shock crossing location), and 38.0 and 43.0 (downstream of the shock crossing location). The fin leading edges are at $x/\delta_\infty = 0$. The shock crossing location is at $x/\delta_\infty \approx 34.0$. On each plane, a local coloring scheme is employed in order to elucidate important flow features such as shocks, compression, and expansion regions. Thus, for any given plane, the colors blue through red represent minimum through maximum values of static pressure, respectively, *on that plane.*

Figure 5a displays the shock structure associated with the individual fin interactions. The primary, secondary, and rear shocks, described by Alvi and Settles,[23] are clearly observed. The separation shocks associated with the individual fin interactions meet at approximately $x/\delta_\infty = 25.0$ as indicated by the centerline surface pressure (Fig. 3a). The initial stage of the interaction of the separation shocks at $x/\delta_\infty = 28.0$ is shown in Fig. 5b. In the region between the initial intersection of the separation shocks ($x/\delta_\infty = 25.0$) and the intersection of the primary shocks ($x/\delta_\infty = 34.0$), a new shock system is formed near the surface (Fig. 5c) at $x/\delta_\infty = 33.0$. This shock system displays a "$\cap$" shape, forming a high-pressure region near the centerline upstream of the interaction of the primary shocks. Downstream of the interaction of the primary shocks, an expansion region forms between the two reflected shocks (Figs. 5d and 5e). The highest pressures are located above the plate and the surface pressure continues to increase towards the inviscid level with increasing downstream distance. The description of the overall shock structure is, however, incomplete, due to the limitations imposed by the shock-capturing nature of the numerical algorithms, and continued collaborative experimental and computational research is needed to elucidate further details.

Outflow Nonuniformities

The successful design of high-speed inlets depends heavily on the effective control of three-dimensional turbulent interactions in order to minimize total pressure losses and to obtain nearly uniform flow. Given the complexity of the flow physics of such interactions, it can be expected that even simplified geometries such as the crossing shock configuration have significant nonuniformities in the outflow.

Figures 6 and 7 show contours of Mach number and total pressure (P_t/P_{t_∞}) on two typical cross-flow (y-Z) planes for the flowfield computed using the Baldwin-Lomax model. Comparable results were obtained for the k-ϵ model. The planes are at $x/\delta_\infty = 23.0$ and 43.0, which are upstream and downstream of the shock crossing location, respectively. At $x/\delta_\infty = 23.0$, the Mach number and total pressure distributions are, as expected, similar to that observed for single-fin interactions. The contours at $x/\delta_\infty = 43.0$ show the accumulation of low Mach number (and low total pressure) fluid near the interaction centerline as a consequence of the interaction of the two individual vortical structures. As observed in the discussion on the flowfield streamline structure, the core of this low Mach number/total pressure region is formed by the low energy streamlines originating from deep within the upstream boundary layer, e.g., at $y/\delta_\infty = 0.01$. Away from the centerline, there is a gradual increase in Mach number and total pressure to the local freestream values. This is associated with the fluid with originating at higher y/δ_∞ levels (and consequently having higher energy) within the upstream boundary layer.

Conclusions

The interaction between crossing oblique shocks generated by two symmetric sharp fins with the turbulent boundary layer on a flat plate at a Mach number $M_\infty = 2.95$ and Reynolds number $Re_{\delta_\infty} = 2.5 \times 10^5$ has been investigated theoretically (numerically) and experimentally for fin angles of $(\alpha_1, \alpha_2) =$ (11 deg, 11 deg). The full three-dimensional mean compressible Reynolds-averaged Navier-Stokes equations are solved, with the effects of turbulence incorporated through either the Baldwin-Lomax algebraic eddy-viscosity model or the Jones-Launder two-equation model. The following conclusions are reached:

1) The mean surface pressure distributions predicted by the computations using the two different turbulence models are in general agreement with experiment. The extent of upstream influence is underpredicted by both models with a maximum underestimate of 2.0–2.5δ_∞ at the centerline of the interaction. The computed spanwise pressure distributions downstream of the shock crossing location display a more peaked profile than observed in the experiment. The computed surface streamline patterns indicate "separation" of the flow (based on the criteria of Lighthill).

2) The principal feature of the flowfield streamline structure is the "collision" of two slowly counter-rotating vortical structures generated as a result of the initial independent shock wave boundary-layer interactions due to the fins. The vortical structures are formed by streamlines originating from deep within the upstream boundary layer.

3) Associated with the vortical-structure collision is the formation and subsequent growth of a low Mach number/low stagnation pressure region downstream of the shock crossing location, indicating significant nonuniformity in the outflow. This result has important implications to the design of high-speed inlets.

4) The study has yielded a "first look" at the overall flowfield structure of the interaction. Further computational and experimental studies are in progress in order to elucidate the full details.

Acknowledgments

This research was sponsored by the Air Force Office of Scientific Research under Air Force Grants 86-0266 and 89-0033 monitored by Len Sakell. Supercomputer resources were provided by the National Science Foundation at the John von Neumann Center and by the NASA Ames Research Center. Analysis of the flowfield data sets was performed at the Rutgers-College of Engineering Supercomputer Remote Access Center supported by Rutgers University.

References

1 Settles, G., and Dolling, D., "Swept Shock/Boundary Layer Interactions—Tutorial and Update," AIAA Paper No. 90-0375, Jan. 1990.

[2]Zheltovodov, A. A., Maksimov, A. I., and Shilein, E. K., "Development of Turbulent Separated Flows in the Vicinity of Swept Shock Waves," *The Interactions of Complex 3-D Flows,* edited by A. M. Kharitonov, Inst. of Theoretical and Applied Mechanics, USSR Academy of Sciences, Novosibirsk, Russia, 1987, pp. 67–91.

[3]Gaitonde, D., "Numerical Investigation of Some Control Methods for 3-D Turbulent Interactions Due to Sharp Fins," AIAA Paper 89-0360, Jan. 1989.

[4]Mee, D. J., "Experiments Involving the Interactions of a Turbulent Boundary Layer with Single and Intersecting Fin-Induced Swept Shock Waves and Swept Expansion Fans," Dept. of Mechanical Engineering, Univ. of Queensland, TR 11/86, Australia, 1986.

[5]Lighthill, M., "Introduction. Boundary Layer Theory," *Laminar Boundary Layer,* edited by L. Rosenhead, Oxford Univ. Press, Oxford, England, UK, 1963, pp. 72–82.

[6]Batcho, P. F., Ketchum, A. C., Bogdonoff, S. M., and Fernando, M., "Preliminary Investigation of the Interactions Caused by Crossing Shock Waves and a Turbulent Boundary Layer," AIAA Paper 89-0359, Jan. 1989.

[7]Sun, C. C., and Childs, M. E., "A Modified Wall Wake Velocity Profile for Turbulent Compressible Boundary Layers," *Journal of Aircraft,* Vol. 10, No. 6, 1973, pp. 381–383.

[8]Narayanswami, N., Knight, D., Bogdonoff, S. M., and Horstman, C. C., "Crossing Shock Wave-Turbulent Boundary-Layer Interactions," AIAA Paper 91-0649, Jan. 1991.

[9]Rubesin, M., and Rose, W., "The Turbulent Mean Flow Reynolds-Stress and Heat Flux Equations in Mass Averaged Dependent Variables," NASA TMX 62248, March 1973.

[10]Baldwin, B., and Lomax, H., "Thin Layer Approximation and Algebraic Model for Separated Turbulent Flows," AIAA Paper 78-257, Jan. 1978.

[11]Knight, D., Horstman, C., Shapey, B., and Bogdonoff, S., "The Flowfield Structure of the 3-D Shock Wave Boundary Layer Interaction Generated by a 20-deg Sharp Fin at Mach 3," *AIAA Journal,* Vol. 25, No. 10, 1987, pp. 1331–1337.

[12]Jones, W., and Launder, B., "The Prediction of Laminarization with a Two-Equation Model of Turbulence," *International Journal of Heat and Mass Transfer,* Vol. 15, 1972, pp. 301–304.

[13]Knight, D., "A Hybrid Explicit-Implicit Numerical Algorithm for the Three-Dimensional Compressible Navier-Stokes Equations," *AIAA Journal,* Vol. 22, 1984, pp. 1056–1061.

[14]MacCormack, R. W., "Numerical Solution of the Interaction of a Shock Wave with a Laminar Boundary Layer," *Lecture Notes in Physics,* Vol. 8, Springer-Verlag, Berlin, 1971, pp. 151–163.

[15]Keller, H., "Accurate Numerical Methods for Non-Linear Two Point Boundary Value Problems," *SIAM Journal of Numerical Analysis,* Vol. 11, 1974, pp. 305–320.

[16]MacCormack, R. W., "A Numerical Method for Solving the Equations of Compressible Viscous Flow," *AIAA Journal,* Vol. 20, No. 9, 1982, pp. 1275–1281.

[17]Knight, D., "Calculation of 3-D Shock Turbulent Boundary Layer Interaction Generated by a Sharp Fin," *AIAA Journal,* Vol. 23, No. 12, 1985, pp. 1885–1891.

[18]Horstman, C., and Hung, C., "Computation of Three Dimensional Separated Flows at Supersonic Speeds," AIAA Paper 79-0002, Jan. 1979.

[19]Horstman, C., "Computation of Sharp Fin Induced Shock Wave-Boundary Layer Interactions," AIAA Paper 86-1032, May 1986.

[20]Knight, D., Raufer, D., Horstman, C. C., Ketchum, A., and Bogdonoff, S., "Supersonic Turbulent Flow Past a 3-D Swept Compression Corner at Mach 3—Part II," AIAA Paper 88-0310, Jan. 1988.

[21]Knight, D., Horstman, C., and Settles, G., "Three-Dimensional Shock Wave-Turbulent Boundary Layer Interactions Generated by a Sharp Fin at Mach 4," AIAA Paper 91-0648, Jan. 1991.

[22]Knight, D., and Badekas, D., "On the Quasi-Conical Structure of the Swept Shock Wave-Turbulent Boundary Layer Interaction," AIAA Paper 91-1759, June 1991.

[23]Alvi, F. S., and Settles, G. S., "Structure of Swept Shock Wave/Boundary Layer Interactions Using Conical Shadowgraphy," AIAA Paper 90-1644, June 1990.